Cellular internalization of Godanti Bhasma (anhydrous $CaSO_4$) induces massive cytoplasmic reversible vacuolation and survival response of mammalian cells.

Achariya Balkrishna* 1 Subrata K. Das 1,2 * #, Alpana Joshi 1,3, Vinamra Sharma 1,4, Laxmi Bisht 1, Neeladrisingha Das 5, Niti Sharma 1, Sunil Shukla 1, Deepika Mehra 1, Kamal Joshi 1 and Santanu Dhara 2.

Author's Affiliation:

1- Drug Discovery and Development Division, Patanjali Research Institute, Patanjali Research Foundation Trust, NH-58, Haridwar-249405, Uttarakhand, India.

2- School of Medical Science and Technology, IIT Kharagpur-721302, India.

3- Shobhit University, NH 58, Meerut- 250110, India.

4- Amity University, Noida- 201313, India.

5- Department of Biotechnology, IIT-Roorkee, Roorkee-247667, India.

***** Both authors made equal contributions

Address correspondence to subratakdas09@gmail.com

Abstract

Cellular internalization and intracellular trafficking of particles depend on their specific physicochemical properties. Godanti Bhasma (GB) is a traditional Indian medicine formulation prepared by heating of gypsum powder with herbal extracts. Chemically, GB is anhydrous calcium sulfate. During formulation it obtains unique physicochemical properties that lead to its rapid cellular internalization and induction of massive cytoplasmic vacuolation. Interestingly, no cellular internalization was found with parent gypsum particle. Flow cytometry analysis and live tracking of GB treated cell showed particle internalization, vacuole formation, particle dissolution and later vacuolar turnover. GB particle dissolution in acidic cell free solution mimics intravacuolar environment where GB was disintegrated under acidic pH suggesting lysosomal enzymes might have no role in GB degradation. Vacuolation often accompany with the sign of cell death whereas, in our study, massive vacuolation by GB did not induce any cell death. Moreover, GB treated cells survive with complete vacuolar process, which was reversed following post-treatment with vacuole inhibitors in GB treated cells, suggesting normal vacuolar function is essential for cell survival. In immunoblotting, upregulation of LC3-II was found in GB treated cells. Treatment of the cells with GB was also found to induce translocation of the LC3 protein from the nucleus to vacuolar membrane by immune-cytochemistry, indicating LC3 associated phagocytosis (LAP) like function. This was found to be reversed in the cells treated with vacuole inhibitors. The vacuolar function essential for cell survival, preserves mechanistic correlation with LC3 lipidation on vacuolar membrane, intracellular controlled and slow degradation of GB particle and further vacuolar turnover limiting swelling pressure in cells.

Keywords: Gypsum, Anhydrous calcium sulfate, Phagocytosis, Vacuole biogenesis, Lysosomal activity, Particle degradation.

Introduction

Eukaryotic cells develop intracellular membrane-bound organelles that compartmentalize biochemical and biophysical processes essential for cellular functions. Cytoplasmic vacuoles are one member of the organelles that serves a variety of functions including; secretory, excretory, and storage. Unlike plant and fungi cells, most animal cells commonly do not contain vacuoles as regular organelles. The vacuoles in animal cells are very smaller than plant and fungi, enriched with hydrolytic enzymes called lysosome. These are about 0.2-2 μm in diameter and acidic in nature. Irreversible cytoplasmic vacuolization has been found in animal cells, when cell is infected by some viral and bacterial pathogens [1-4] as well as with the treatment of various natural and artificial low-molecular-weight compounds including medicinal drugs and industrial pollutants [5-11]. In most of the cases, irreversible cytoplasmic vacuolation is related to cell toxicity. In contrast to irreversible vacuolation, reversible vacuolation occurs as long as chemical compounds are present in medium suggesting vacuolization is a reversible process. But prolonged exposure of the chemical causes vacuole irreversible and eventually cell death [12-14].

Vacuolation is initiated by the interaction of cell membrane and particles. Researchers have tried to understand the response of the biological system during and after particle uptake in different cells and tissue model [15-17]. The mechanism of particle uptake occurs either by diffusion or endocytosis. Endocytosis is a process where extracellular or cell surface particle is internalized by the invagination as well as pinching off the plasma membrane. Usually, larger particles (>0.5 μm) internalized by phagocytosis that occurs in restricted cells (macrophage, monocyte) [18]. However, internalization of the larger particle by non-professional-phagocytic cells is also reported [19-21]. Phagocytosis is triggered by the interaction of the particle-bound ligand with receptors on the surface of the cell membrane; then the particle is delivered into a sealed intracellular vacuole i.e. phagosome [22-24]. The nascent phagosome matures by interaction either with endosomal vacuoles or lysosomes or both to develop phagolysosome hybrids enabling the transfer of lysosomal hydrolytic enzymes that mediate degradation of vacuolar cargo [25-27]. V-ATPase delivered from the membranes of the endocytic pathway during phagolysosome formation is responsible for the maintenance of acidification in the vacuolar lumen [28, 29]. The maintenance of acidification in the vacuolar lumen is crucial for the hydrolytic activity of the lysosomal enzymes. Various unwanted biomolecules including

proteins, nucleic acids, carbohydrates, and lipids are broken down by the hydrolytic enzymes in an acidic condition in the vacuolar lumen. The strategy of vacuole biogenesis in response to extracellular particle, and its further structural and functional maintenance is very important for the survival of cells. When the vacuolar function is impaired, cells become stressed and eventually cell death occurs. However, a precise mammalian cell-based model system for phagocytic pathway has not yet been discovered.

For the first time, vacuole biogenesis in mammalian cell (non-phagocytic) was observed by one of the traditional Indian drug named Godanti Bhasma (GB). Bhasmas are unique Ayurvedic medicines, prepared by incineration of metals or minerals particles processed with the herbal extract [30]. In India, therapeutic uses of these medicines are commonly evidenced since the 7^{th} century [31]. GB is a traditional ayurvedic medicine for digestive impairment, headache, chronic fever, cough, dyspnoea, phthisis leucorrhoea and emaciation in children [32, 33]. It is also used in migraine [34], osteoarthritis [35] and gastric ulcer [36]. However, the mechanism of action of the drug has yet not been studied.

In the present study, we assessed *in-vitro* cell-based assay to know how cells interact with GB particle and following mechanism of vacuole biogenesis and internalized particle degradation.

Results

Godanti Bhasma; Anhydrous phase of gypsum

In Ayurveda, incineration procedure plays an important role in transformation of metals or minerals into therapeutic form. In the present study, GB is prepared through incineration of gypsum powder at 800 °C temperature. Here we characterized the structural difference of gypsum and GB particle by using Confocal Raman in the range of 20-4000 cm^{-1}, and FT-IR in the range of 600-4000 cm^{-1}. Both vibrational spectroscopy techniques are versatile in probing structural changes and dehydration in minerals. In Raman spectroscopy (Fig. 1A), the presence of water in gypsum was detected by its two characteristic absorption bands at 3494 and 3406 cm^{-1} regions showing O-H stretching mode of gypsum which was disappeared in the GB (anhydrite phase). The formation of phase wise anhydrite forms of $CaSO_4$-H_2O system was confirmed by the complete disappearance of water molecules while heated at 110 to 1300°C [37]. Further, the main Raman band centered at 1008 cm^{-1} in gypsum was shifted to 1017 cm^{-1} in GB. These are υ1 symmetric stretch vibration modes of SO_4, up-shifted following the alteration of the hydration

degree. Both compounds exhibited doublet for υ2 symmetric bending of SO_4 at 415, 494 cm^{-1} and 416, 497 cm^{-1} in gypsum and GB, respectively. The peaks at 1136 cm^{-1} in gypsum were bifurcated at 1127, 1158 cm^{-1} in GB revealed SO_4 in υ3 asymmetric stretch vibration modes. The peaks observed at 619 and 671 cm^{-1} in gypsum and 608, 625 and 674 cm^{-1} in anhydrite gypsum are υ4 (SO_4) asymmetric bending vibration modes. All these observations strongly indicate structural changes involving the rearrangement of sulfate ions and O-H stretching during the transition of gypsum to GB with an onset temperature at 800 °C. The details of Raman spectra of gypsum and GB are summarized in Table S1 comparing the observed internal modes made between $CaSO_4$-H_2O system (hydrous to anhydrite phases). Some Raman spectra observed at 129, 177cm^{-1} in gypsum and 126, 168cm^{-1} in GB were attributed to Ca ion. The thermal transformation of gypsum was studied extensively by many authors [38-40].

The FT-IR spectrum of gypsum centered at 3527 and 3387 cm^{-1} was assigned to O-H bending vibrations, and the band at 1679 and 1617 cm^{-1} corresponds to O-H anti-symmetric stretching indicates crystalline water molecules in gypsum which were disappeared in anhydrous GB. The band at 1091 cm^{-1} in gypsum and 1097 cm^{-1} in GB associated with the stretching vibrations mode of the sulfate (SO_4) [40] (Fig. S1).

Surface morphology and elemental composition of GB particle were analyzed by FESEM and EDX, respectively. The SEM analysis demonstrated the irregular shape with different size of GB particles ranging mean size of 0.5−5 μm (Fig. 1B and 1D). The EDX was used to detect elemental composition of Bhasma particle as calcium sulfate (Fig. 1C).

Zeta potentials were measured to evaluate electrochemical changes at the microparticle surface due to the thermal transformation from gypsum to GB. Gypsum microparticles showed a negative Z potential -10.42±0.98 and -11.1±0.45, whereas GB particles altered the surface charge towards neutral -1.33±2.65 and -1.75±2.41 in 10% FBS and water suspension, respectively. However, near to neutral zeta potential of particles tend to aggregate faster due to the less physical stability of the colloidal systems [41].

Godanti bhasma induced massive vacuolation in cells

In the present study, we observed massive vacuolation in the cytoplasm with various sizes of the vacuole in 3T3-L1 cells exposed to the GB (Fig. 2B & S3), whereas raw gypsum powder was unable to induce any vacuolation (Fig. 2C). The vacuoles were stained with neutral red

indicating their acidic nature (Fig. 2D). As pH in lysosome and vacuoles are lower than the cytoplasm, the dye penetrates inside vacuole, becomes charged and retained inside the lysosomes and vacuoles. Quantification of GB induced vacuolation was done by neutral red uptake assay in cells. A dose-dependent response was observed in 3T3-L1 cells exposed to GB with various concentrations, the vacuolation increased gradually according to the gradual increasing concentration of bhasma particles (Fig. 2G). In time course experiment, vacuolation was increased up to 24 h of bhasma treatment (Fig. 2H). It is also noted that nascent vacuoles first appeared around the perinuclear region within 2-3 hours of GB treatment, and a gradual increase in the number and size of vacuoles was observed until much of the cytoplasm occupied by a single or several vacuoles (Fig. S2). In our experiment, the bhasma particles were precipitated due to the gravitational force on the surface of the cell. However, the vacuoles were formed as long as particles are available in the culture medium. The size of vacuole approximately 1–70 µm in diameter was observed after 24 h of bhasma treatment (Fig. S3). To the best of our knowledge, extraordinarily large vacuoles were shown to induce in mammalian cells.

It was shown that GB induced vacuole formation was inhibited by Bafilomycin A1 (BFA1) indicating vacuolation require V-ATPase enzymes (Fig. 2E) that supply H^+ to vacuole from cytoplasm. Further we found that Chloroquine (CQ) was also inhibited GB induced vacuolation (Fig. 2F). CQ is a lysosomotropic weak base; it diffuses into lysosome and vacuole where it becomes protonated and trapped. The protonated CQ then increases the vacuolar pH. The kinetic study of GB induced vacuolation was also done to identify the minimal concentration of two lysosomal-vacuolar inhibitors (BFA1 and CQ) required to block the vacuolation process in 3T3-L1 (Fig. 2I and 2J). The vacuolation was suppressed up to 120 nM of BFA1 whereas, vacuolar size and number was found to increase gradually up to 2 nM concentration. In all the above tested concentrations, cells showed 100% viability. In the case of CQ treatment, GB induced vacuolation was suppressed up to 2 µM concentration, gradual vacuole size was shown to increase in lower concentrations up to 0.5 µM.

To see the specificity and degree of the vacuolation, we examined total of seven cell lines 3T3-L1, Neuro 2a, A549, MDA-MB231, MCF-7, HCT-116, and HeLa. Interestingly, all the non-phagocytic cells exhibited a similar pattern of vacuolation after 24 h of GB treatment (Fig. S 4).

Cellular internalization of GB particle

Initially FESEM was used to identify the vacuole and particle inside the vacuole within cells. FESEM analysis clearly showed the presence of complete vacuole and particle inside of it (Fig. S5 A&B), but EDX did not show any spectral change as EDX was not able to detect in intact cells. To know the elemental analysis of particle inside the vacuole, we performed transverse sections (10 µm) across the fixed cells to expose the particles, and then further cell was analyzed through FESEM and EDX. The results clearly indicated that vacuole contains particle composing calcium, sulfur and oxygen elements which were confirmed through FESEM as well as EDX spectra of sectioned cells. These elements correspond to the GB particle inside the vacuole (Fig. S5 C&D).

We investigated the internalization of GB particle in cells by flow cytometer analysis (Fig. 3). Cells were incubated with bhasma particles at different time points starting from 30 min to 12 h. The pictures showed that particles were localized on the surface of cells at 30 min of treatment (Fig. 3B). Membrane invagination was found at the site of particle attachment on the surface of the membrane and after its attachment a circular extension or curvature of the membrane was observed around the surface of the attachment which might be the phagocytic cup formation (Fig. 3C). The phagocytic cup was studied extensively by many authors [23, 42, 43]. After internalization, particles were associated with membrane-enclosed vacuoles presumably trafficking to the endocytic vacuolar system. It was clearly found that the size of vacuoles increased over time (Fig. 3D).

GB Particle degradation inside the vacuole

To know the GB particle degradation, flow cytometry analysis of isolated particles from cell lysate was done at different time points (1 to 24 h) of GB treatment in 3T3-L1 cells (Fig. 4A). The result revealed that most of the particles were associated with cells at 1 h of GB treatment. The particles at this stage were fully internalized or going to be internalized. However, 1 h culture media contains a certain amount of particles which were not internalized. The particle internalization in cells is a continuous process according to the availability of particles in the culture media. In the same figure, it is clearly shown that the particles were internalized and further degraded over times up to 24 h. Particles were completely degraded by cells and no

particles were available in culture media after 24 h. It seems that the sample with GB treatment at 24 h was same as samples of untreated control cells.

The particle degradation inside the vacuole was also confirmed by time-lapse microscopy targeting a single cell (Fig. 4B). It was clearly found that the particle was degraded into smaller particle over time and finally disappeared from the vacuole. In supporting information Movie-1 we found that most of the particles were rapidly internalized by 3T3-L1 over the first 1-3 h of incubation. Co-treatment of GB with either BFA1 or CQ inhibits vacuolation process. It was clearly found that in the presence of inhibitor, GB particles were attached on the surface of the membrane but not internalized as further acidification was stopped. Therefore following internalization of the particle, acidification is required to make vacuole. After the disappearance of particle the vacuoles were also decreased in size over time and finally disappear from cytoplasm restoring the normal morphology of cells (Fig. 4B and Movie 1)

Bhasma particles degradation is associated with lysosomal activity inside the vacuole

Lysosomes contain many hydrolytic enzymes such as nucleases, proteases, and lipases. The hydrolytic enzymes require an acidic environment for their optimal activity, and lysosome provides this by maintaining low pH in its interior. In eukaryotes, lysosomes allow vacuolar digestion by fusing with endocytic vacuoles (endosomes and phagosomes) [25-27]. The H^+ pump (V-ATPase) in the lysosomal membrane, as well as endocytic vacuoles, uses the ATP to pump H^+ into the vacuolar lumen, thereby maintaining the lumen at its acidic pH [28,29]. Acridine orange (AO) is a pH indicator in live cells, it emits red fluorescence at acidic pH and green fluorescence at physiological pH. We used acridine orange to monitor intracellular pH in vacuoles in cultured cells at different time points of GB treatment (Fig. 5A). At 1 h of particle addition, AO was detected mainly in the perinuclear region as small lysosomal compartments. At 3 h of treatment, AO stained in round shaped granular structure in the perinuclear region of cells. This indicated that the granular structure is the endocytic vacuoles which are acidic in nature. At 12 and 24 h, the vacuoles were huge and also emit red fluorescence. The GB particles inside the vacuoles might have a possibility of degradation directly in the vacuolar acidic environment. However lysosomal degradation is done by lysosomal hydrolytic enzymes in acidic condition.

Mimicking vacuolar pH environment in cell-free environment

The dynamic process of vacuole biogenesis involves particle internalization, phagosome formation, fusion of endocytic pathway, and finally phagolysosome formation. The pH of these vacuolar organelles ranges from 6.5-5.0, while pH of the primary lysosome is 4.5 [20, 44, 45]. We examined the solubility of GB under physiological conditions (pH 7.4) to vacuolar/lysosomal acidic conditions (pH 4.5) in cell free environment. GB particles were incubated in different pH condition (4.0-7.5) of PBS buffer solution, and turbidity test (580 nm) was done in time points 15 min, 90 min, 3, 6, 12 and 24 h (Fig. 5B). In the buffer solution of pH 7.5, GB maintained their original size indicating that GB was insoluble at physiological conditions. By contrast, GB was disintegrated under acidic conditions at a pH value similar to phagolysosomes. This size of GB particle at physiological conditions was larger where these particles were dissolved under acidic conditions (Fig. 5C), which is consistent with the assumption that particle was degraded to a smaller size in vacuole because anhydrous calcium sulfate shows solubility at pH range 4-6.

Godanti Bhasma induced vacuolation does not affect cell viability and proliferation

Initially, 3T3-L1 cells were treated with different concentrations (0-2.5 mg/ml) of GB for a period of 24 h to test its effect on cell viability. After endpoints, no significant signs of toxicity were observed in all tested concentrations of GB in 3T3-L1 cells (values over 100% should be considered as complete viability). Further, the effect was examined after the 48, 72 and 96 h of treatment on the cell viability of 3T3-L1 (Fig. 6A) and it was not found toxic to the cells. To explore the cytotoxic effects of GB at various concentrations (0-2.5 mg/ml) in six other cells lines (Neuro 2a, A549, MDA-MB231, MCF-7, HCT-116, and HeLa), cells were analyzed after 24 h of treatment; no toxicity was observed (Fig. 6B). Furthermore, the effects of GB on cell proliferation were investigated using *in vitro* scratch assay. The cell-free scratch area in control, as well as GB, treated 3T3-L1 cells were closed at 8 h post-scratch **(**Fig. 6C**)**. This finding clearly indicated that GB does not cause any significant effect on cell viability as well as cell proliferation.

Activation of the caspase-3 pathway is a characteristic of apoptosis, and to determine the involvement of caspase-3 in GB induced vacuolation, the activation of caspase-3 by colorimetric caspase-3 assay system at different time points was examined. Exposure of 3T3-L1 cells to Bhasma particles (0.15 mg/ml) for 0, 2.5, 5, 10 and 24 h caused no increase in caspase-3 activity

compared to a positive control (caspase-3). Untreated cells were used as a negative control (data not shown).

Post treatment of vacuole inhibitors BFA1 and CQ promote cytotoxicity in GB induced vacuolated cells

In our experiment, we found that GB induces massive vacuolation without any cell death. The vacuoles were reversible as particles were degraded and following vacuolar turnover. To prove the vacuolar function in survival of GB induced vacuolated cells, we introduced vacuole inhibitor BFA1 (100nM) and CQ (1μM) after 24 hours of GB treatment in 3T3-L1 cells. We performed cell toxicity assay after 48 hours of the inhibitors addition, and found a significant cell death in GB+BFA1 (Fig 6D) and GB+CQ (Fig 6E) compared to respective controls. The result indicated that cell death occurs due to irreversible or defective vacuole by inhibition of vacuolar function with the post treatment of the vacuole inhibitors.

GB induced vacuolation is associated with LAP like function

LC3-associated phagocytosis (LAP) is a phenomenon distinct from autophagy, wherein LC3 translocation occurs to particle containing phagosome. To identify the LAP-like LC3 lipidation, we performed immunocytochemistry with LC3A/B antibody in GB induced vacuolated cells (Fig. 7A and S6). The result indicated that LC3 protein is accumulated in the nucleus of untreated cells, whereas in GB treatment it translocated to the membrane of vacuoles, suggesting activation of LAP like function in GB induced vacuolated cells. However, cytoplasm and nucleus also stained with LC3 antibody. To understand the relation between LAP like function and vacuole inhibitor BFA1 in GB treated cells, post treatment of BFA1 (100nM) was done in GB induced vacuolated cells for 18 h. We found that the accumulation of LC3 (lipidated LC3) was suppressed on the vacuolar membrane/periphery, whereas LC3 expressed in whole cell. The present findings indicated that the LC3 protein have an important role in GB induced vacuolar function through LAP like mechanism. Also, we estimated LC3 expression in cell lysate of 3T3L1 in different time points after GB addition compared to untreated control and CQ treatment (autophagy inhibitor) (Fig. 7B). The expression of LC3 increased in GB treated samples compared to untreated control where as in CQ it was highly expressed. The result indicated that the expression of LC3 is in steady state in GB treatment suggesting LAP like

function involved in vacuolar process. However, in CQ treatment autophagosome accumulation is enhanced due to inhibition of Autophagy flux. To understand the role of vacuole inhibitors in LAP machanism, we examined LC3 expression with GB, BFA1 and CQ alone and GB combined with post BFA1 or CQ treatment in 3T3L1 cells by western blotting (Fig. 7C). The cell lysates were prepared after 18 h of BFA1/CQ treatment. We found that LC3 was highly expressed in presence of BFA1 and CQ with or without GB treatment. Whereas moderate LC3 expression was found in only GB treatment compared to untreated control. We also performed the same experiment in Neuro 2a cells (Fig. 7D), and found that the same expresion pattern as of 3T3L1 cells. The result indicated that LAP like machanism is functional in vacuolated cells wherein it is abolished with the post treatment of vacuole inhibitors.

Discussion

The present study sheds lights on the vacuole biogenesis induced by Godanti bhasma (GB) and downstream vacuolar progression in animal cells. In this study, the most interesting phenomenon is that massive vacuolation was observed in mammalian (non-phagocytic) cells with the treatment of GB (an anhydrous $CaSO_4$), whereas parent gypsum (dihydrate $CaSO_4$) did not induce any vacuolation. To know this phenomenon, initially we analyzed the structural changes in gypsum and GB. The change of crystal structure on heating of gypsum was clearly evaluated by Raman and FT-IR spectroscopy. Complete removal of water molecules from dihydrate gypsum makes it more condensed crystalline form (orthorhombic anhydrite) [46] that promote their bioavailability to animal cells. According to Ayurvedic pharmaceutics, an ideal heating of inorganic minerals is essential for required physicochemical changes during Bhasma formulation [47]. The present finding supports the ancient concept of the Bhasma formulation.

Surface charge of particle is an important factor for cellular internalization. It is obvious that the interaction between positively charged particles with negatively charged cell membrane increase cellular uptake [48, 49]. It is interesting to observe from our experiments that gypsum which is near to neutral charge was not capable to induce vacuole formation while neutral charged GB particle induced vacuolation effectively. Therefore, our present study reveals that charge is not an important factor for cellular internalization of GB particle.

The possible reason of such internalization of GB particles might be its structural rearrangement that facilitated to recognize cell surface receptors and, thus permeating into cells by receptor-mediated cellular uptake. Receptor-ligand interaction during phagocytosis is well studied, Fcγ *receptors* which recognize particles coated immunoglobulin *G* is the most widely studied example of phagocytosis [24]. However, few studies have been reported on the interaction of particle-bound ligand-receptors of non-phagocytic cells. The life-threatening human pathogen *Staphylococcus aureus* have an ability to internalize in a variety of non-phagocytic cells like epithelial, endothelial, fibroblast, osteoblast cells etc. The pathogen uses α5β1 integrin receptor, chaperons and the scavenger receptor CD36 to internalize into target host cells [50]. *Gratton et al* [19] revealed that HeLa cell internalized PRINT particle of 1-3 μm by several different mechanisms of endocytosis. However, the extensive study will be needed to understand the interaction between GB particle bound ligand and cell surface receptors, and downstream molecular mechanism.

Flow Cytometry images revealed phagocytic cup formation at the time of particle internalization. The phagocytic cup formation is well established by many authors [23, 42, 43]. After particle internalization, the nascent vacuoles appeared around the perinuclear region and a gradual increase in the number and size of vacuoles was observed until much of the cytoplasm occupied by a single or several vacuoles. The nascent vacuole fused with lysosome, transferring lysosomal contents to become phagolysosomes. Our experiment revealed that GB induced vacuolation required V-ATPases. V-ATPase supply high concentration of H^+ leading higher osmotic pressure within vacuoles, and thus resulting in large vacuole due to the influx of water molecules [51-53]. V-ATPases are found on the membranes of intracellular vacuolar organelles, like endosomes, lysosomes, and phagolysosomes [25,26].

Further flow cytometry analysis of cell lysate indicated that the internalized particles were found to be degraded slowly. The degradation was also clearly confirmed by time lapse microscopy targeting single cell with intravacuolar GB particle. The intracellular degradation of GB particles observed in endocytic vacuoles was due to its acidic environment. In our study, the vacuolar acidic environment was broken with the treatment of BFA1 and CQ, resulting inhibition of vacuole progression and following particle degradation. Increasing of luminal pH of vacuole also blocks the fusion of phagosomes and late endosomes [28]. However, BFA1 and CQ induce autophagic vacuole in cells have been well studied [54,55]. In our study, we found that GB

particle was degraded in cell free environment having pH 5-6 which mimics vacuole-lysosomal pH. We calculated time taken for bhasma particle degradation in cell free environment and vacuolar lumen of 3T3L-1 cells. We found that in cell free condition, particle digestion was taken 10 h at pH 5, 24 h at pH 5.5 and more than 24 h at pH 6 whereas, in cellular system it took less than 24 h for complete degradation. In the video, targeting single cell with intravacuolar particle, we also found that the bhasma particle degraded at 8 h. These phenomena indicated that the acidic environment inside the vacuole might be the reason for particle degradation. However, lysosomal enzymes are activated in the acidic pH to break down various cellular and non-cellular components. Lundborg et al 1984 [56] suggested that metal particles dissolve in the alveolar macrophages might be due to the reduced pH in the phagosomes. Therefore, our findings indicated that lysosomal enzymes might have no role in the GB particle degradation.

GB induced vacuolated cells was normal in proliferation which was evident by MTT and cell migration assay. These findings clearly indicated that GB does not cause any significant effect on cell toxicity as well as cell proliferation. The vacuolation is the sign of cell death in most of the cases by triggering apoptotic or non-apoptotic pathway [57-62]. Initially, it was assumed that the accumulation of vacuoles in cell cytoplasm hampers cell functions and cause cell death. The mechanisms of cell death have been studied by many authors, mainly not due to vacuolation but through disruption of mitochondria, endoplasmic reticulum, Golgi apparatus, and endo-lysosomal system [8, 59, 63-65]. Moreover, the cell protects itself from a toxic substance by developing vacuole to separate from the cytoplasm. In this connection vacuolation in cells is an adaptive physiological response, presumably for damage limitation. Where damage limitation fails, cells usually die quickly. In our experiment, post treatment of BFA1 and CQ in vacuolated cells by GB showed a significant cell death compared to GB and BFA1/CQ control. Therefore, it is confirmed that the vacuole inhibitors stopped the vacuolar function by increasing pH in vacuolar lumen and thereby inhibiting further vacuolar progression. The viability loss could include failure to degrade GB particle or persistent of faulty vacuolar organelles. Whereas only GB treated cells survive with active and complete vacuolar process. Also BFA1 and CQ disrupt autophagy flux, leading accumulation of autopagosomes in cells [54, 55]. In the post BFA1/CQ treatment experiment, it can be concluded that excessive accumulation of autophagosome and defective vacuolar function is wasteful process to the cell, there by exerting cell toxicity. In our experiment, the LAP-like LC3 lipidation is activated in GB induced vacuolated cells evidenced

by accumulation of LC3-II on vacuolar membrane whereas LC3 localized in nucleus in untreated cells. This result is strongly supported by the up regulation of LC3 in cell lysate. During vacuolar progression the nuclear LC3 distributed in cytoplasm as soluble LC3-I which in turn conjugated with lipid forming LC3-II and recruited to vacuolar membrane [66-68]. The BFA1 treatment in vacuolated cells disrupts LC3-II accumulation on the vacuolar membrane. Florey et al 2015 [53] suggested that LC3 lipidation is completely blocked by BFA1 treatment. Based on previous report and our current finding, it can be concluded that LAP like function is essential for vacuolated cell survival. Our study indicated a direct evidence of survival strategy of vacuolated cell. The survival response of GB induced vacuolated cells from ions toxicity might be correlated with controlled and sustained release of Ca^{++} and SO_4^{--} due to slow dissociation of GB particle inside vacuole. Perhaps cells get advantages by utilizing the ions for better physiological purpose. Also, cell restored its normal morphology by decreasing vacuolar volume which is associated with cellular protection from potential damaging swelling pressures.

GB is a traditional medicine used in India since a long time for treating mainly digestive impairment, acid-peptic disorders as well as bone-related disorders. Further research will be needed using *in-vivo* as well as *in-vitro* diseases model to evaluate its pharmacological mechanism of action. Also, GB induced vacuole formation in mammalian cells (non-phagocytic) will be a powerful model to study vacuole biogenesis and will undoubtedly identify novel molecular players by manipulating gene of interest.

Materials and methods

Preparation of Godanti Bhasma

For the preparation of GB, initially, raw gypsum was coarsely powdered and washed with warm water. Then, it was suspended in sufficient quantity of lemon (*Citrus limon* L. Osbeck) juice and then subjected to moderate heat (~80 °C) for 90 min. The obtained material was washed with warm water, dried and used for further process. In the next step, the purified powder was placed in an earthen crucible and subjected to Gaja Puta (classics nomenclature used for the quantum of heat) heating in a muffle furnace at ~800 °C for 30 min, and then allowed for self-cooling. The obtained material was further impregnated with Aloe vera (*Aleo barbadensis* Mill.) juice and subjected to another Puta. Finally, white colored Godanti Bhasma is obtained [32].

Characterization of raw gypsum and Godanti Bhasma (GB)

In this study, initially Confocal Raman (WITec Confocal Raman system; model: Alpha300 series), and Fourier-transform infrared (FT-IR) spectroscopic techniques were used to characterize the changes in raw gypsum and GB. Raman images and spectra were recorded using ultra-high-throughput *spectrometer* (UHTS) equipped with a charge-coupled device (CCD) camera, diode laser used for 532 nm excitation, and microscope (Zeiss 100x air objective with numerical aperture 0.9). The FT-IR measurements were obtained at room temperature using AGILENT spectrometer (model: CARY630) equipped with ATR cell attached with Micro Lab PC software. The data was recorded three times from three different set of samples for both experiments.

Further, the surface morphology and particle size distribution of GB sample were observed by Field emission scanning electron microscopy (FESEM) (TESCAN; model: MIRA3) technique. For this sample was anchored on the sample holder, and morphology was probed on selected points to determine elements with the help of detector inbuilt with energy dispersive X-ray analyzer (EDX) (Rigaku; model: XFlash 6I10) at 0-10 keV. Total three different set of particles were examined during scanning. Histograms of particle size distribution were made on three independent FESEM images.

Zeta potentials were measured to evaluate electrochemical changes at the microparticle surface due to the thermal transformation from gypsum to GB. For this samples were suspended in distilled water as

437 well as 10% FBS and surface charged were assessed by zeta sizer nano (Malvern Panalytical, UK,
438 ZS90). Five samples of each set were recorded.
439
440 **Cell Culture**
441 Dulbecco's modified Eagle medium (DMEM), fetal bovine serum (FBS), Antibiotics, Trypsin-
442 EDTA solution were obtained from Thermo Fisher, MA USA. Cell lines (3T3-L1, L6, Neuro 2a,
443 HeLa, HCT-116, A549, MDA-MB231, and MCF7) were procured from National Centre for Cell
444 Sciences (NCCS), Pune, India. The cell was cultured in DMEM (GIBCO BRL, Grand Island,
445 NY, USA) supplemented with 10% inactivated Fetal Bovine Serum (FBS), penicillin (100
446 IU/ml), streptomycin (100 µg/ml) and amphotericin B (5 µg/ml) in a humidified atmosphere of
447 5% CO_2 at 37 °C. The cells were dissociated with Trypsin-EDTA solution. The stock cultures
448 were grown in 25 cm^2 culture flasks, and experiments were carried out in 96- and 6-well plates
449 (Tarsons India Pvt. Ltd., Kolkata, India).
450
451 For cell culture experiment, GB powder (100 mg) was suspended with complete DMEM media
452 (1 ml supplemented with 10% FBS) by vortexing, and leave the tube on a stand for 1 min to
453 settle down larger particle, serial dilution was done using 500 µl of GB suspension. All cell
454 culture experiment (except dose-response experiment) was conducted using 5^{th} dilution of GB
455 suspension.
456
457 **MTT assay**
458 Cell viability was determined using MTT assay in 3T3L1. Cells were seeded (7500 cells/well) in
459 96-well plate and incubated for 24 h. After 24, 48 and 72 h of incubation in presence of GB with
460 serial dilutions (0 – 2.5 mg/ml), the culture medium of each well with or without extract was
461 removed completely from the assay plates and replaced by fresh culture medium (100 µL). MTT
462 (Thiazolyl Blue Tetrazolium Bromide) solution (10 µL of 5 mg/mL), (Thermo Fisher, MA USA)
463 was added into each well to achieve a final concentration of 0.45 mg/mL before incubated for 3 h
464 at 37 °C. After 3 h, the culture medium with MTT was carefully removed followed by addition
465 DMSO (100 µL) (Himedia, India) to dissolve formazan crystals, and then incubated for 1 h
466 before recording the optical density (Envision plate reader, California, USA) at 540 nm. Cell
467 viability test was also performed in six different cell lines (Neuro 2a, A549, MDA-MB231,

MCF-7, HCT-116, and HeLa) at 24 h of culture. The results are presented as the mean ± SD (n=6).

Cell migration assay

Cells were seeded in a 6-well plate ($0.5x10^6$ cells/well), incubated up to 100% confluent. Cells were treated with and without GB. The monolayer of cells was scratched (3 scratches) with a pipette tip after 12 h of treatment, and cells were imaged at 0, 4, 8h post-scratch. The cell-free areas per treatment group were used for analysis.

Caspase assay

The Caspase-3 colorimetric assay was also conducted according to manufacturer instructions (Sigma-Aldrich, MO, USA). 3T3-L1 cells were treated with Bhasma for 0, 2.5, 5, 10, and 24 h. The concentration of the p-nitroanilide (pNA) released from the substrate was calculated from the absorbance values at 405 nm. Three samples were done for each time points.

Crystal Violet staining

Crystal Violet (High Media, India) staining in cells was done for microscopic imaging. Treated cells were washed with 1X PBS, fixed with formaldehyde (10%) for 15 min. After fixation, cells were washed with water and stained with 0.5% (w/v) crystal violet (25% (v/v) methanol) for 25 min, subsequent washing the cells with water until no color was eluted, and images were taken by Bright Field microscope (PrimoVert. Zeiss, Germany).

Neutral Red staining

Relative vacuolation was quantified based on the uptake of the Neutral Red dye (High Media, India) in mammalian cells (Kannan et al. 2014). The experiments were performed in 96-well plates, neutral red (100 µl of 0.5 mg/ml) was added in each well, incubated for 4 h in CO_2 incubator, washed 3 times with PBS, eluted the neutral red by adding destining solution (100 µl containing 50% dehydrated ethanol, 49% deionized water and 1% glacial acetic acid). Neutral Red uptake was determined using a microtiter plate reader (EnVision Multimode plate reader, Perkin Elmer, USA) to measure the absorbance at 540 nm.

Acridine Orange (AO) staining

Cells were grown on glass coverslips, treatment was done for a specific period, the cells were incubated with acridine orange (1 mg/ml) (High media, India) for 15 min at 37 ºC followed by 3 PBS washes, and then immediately observed under a fluorescence microscope (Mantra, PerkinElmer).

Processing of Cells and Its Characterization by FESEM and EDX

Cells were cultured in culture disc up to 70% confluency, GB treatment was done for 18 h after treatment cells were washed 5 times with PBS to remove extracellular particle, cells were trypsinized, centrifuged (1000 rpm for 10 min) to make pellet. Cells were re-suspended in PBS, re-pellet, and replaced with formalin (10%) to fix for 1 h. Cells were replaced sequentially with 70, 95, and 100% ethanol for 1 h each. Treated cells were replaced with xylene (2 times, 1 h) and paraffin wax (2 times, 90 min), refrigerated to set the wax. Wax blocks (containing the cell pellet) were sectioned and selected section was placed on round cover glass, which eventually treated with xylene to remove paraffin and washed (3 times, 5 min each) with PBS. For SEM of fixed cells (without section), cells were also grown on the cover glass, treated with GB particle, fixed with 10% formalin (30 min) and washed 3 times. The processed cells were further characterized through FESEM and EDX stated above. The whole procedure was done from three different samples. Further images of FESEM and EDX was done from each samples.

Cell Preparation for Flow Cytometry

Cells were seeded ($0.2x10^6$ cells/ well) in 12-well plate and cultured for 24 h, GB treatment was done at different time points (30 min, 1h and 12h), washed with PBS (5 times) to removed extra particles, trypsinized and washed again in PBS. The cells were run in Flow cytometer (Amnis® Imaging Flow Cytometers, Millipore, USA). Individual cell images were collected from Flow cytometer image library and analysis was done.

For particle analysis, cells were cultured ($0.2x10^6$ cells/ well) in 12-well plates for 24 h, treatment of GB was done at different time period (1h, 7h, 14h and 24h), culture media were collected in 1.5 ml tubes, the cells were washed with PBS (5 times) to remove particles present in outside of cells, and 500 µl RIPA (20 mM Tris-HCl pH-7.5, 150 mM NaCl, 0.1% Triton X-100, 1% sodium deoxycholate) buffer was added to lyses cell completely. The culture medium

and lysed cell samples containing particle were run in Flow cytometer. Particles suspended in culture media and cell lysate samples were analyzed by the flow cytometer software IDEAS (Amnis Corporation, WA, USA). The two independent experiments were done.

Time Lapse Microscopy

Cells were grown up to 70% confluency in petridish. GB suspension was added into the culture medium and placed the culture dish on stage of imaging microscope (JULI smart fluorescent cell analyzer, Seoul, Korea). The images were captured at every 5 min for overnight. The whole set up was kept in a CO_2 incubator. Movie was made using captured images by software Image J. The time lapse microscopy was done three times.

Different pH Treatment of GB Particles and Turbidity Test

Turbidity is the cloudiness or haziness of a fluid containing particles. 1X PBS solution (2.2 mM KCl, 1 mM Na_2HPO_4, 140 mM NaCl) at different pH (7.5, 7.0, 6.5, 6.0, 5.5, 5.0, 4.5 and 4.0) was made. GB powder (100 mg) was suspended in water, mixed by vortex, and kept in a stand for 1 min to settle down larger particles. Particle suspension (10 µl) was added in PBS (200 µl) of respective pH (n=6) in 96-well plate. The measurement of turbidity was done at different time points (15 min, 90 min, 3 h, 6 h, 12 h, and 24 h) in envision plate reader at 580 nm. The absorbance are plotted (mean ± SD). After 24 h of treatment, images of particle were taken by light microscope (Zeiss, Primovert).

Immunocytochemistry

After treatment, cells were washed with PBS (2 times) and fixed with 4% paraformaldehyde for 15 min. Following three further PBS washes, cells were permeabilized with 0.2% Triton in PBS for 10 min. Cells were blocked in blocking buffer (1% BSA, PBST) for 1h at room temperature and incubated with primary antibody LC3A/B (Thermo Scientific, USA) overnight at 4 °C. Cells were again washed with PBS (3 times, 10 min each), incubated with secondary antibody Goat Anti Rabbit IgG H&L dylight 488 (Thermo Scientific, USA) for 1 h, and then followed by PBS wash (3 times, 10 min each). Only secondary antibody (no primary ab) in treated cells was used as a control. Cells were treated with DAPI (3 g/ml) in PBS for 5 min, wash again with PBS (3 times, 10 min each), Slides were mounted with 50% glycerol. Microscopy was done with

fluorescence microscope (Mantra, Perkin Elmer, USA). The immunocytochemistry was done three times.

Western blotting

Cells were washed with PBS, scraped into ice-cold RIPA (150 mM NaCl, 50 mM Tris-HCl, 1% Triton-X-100, 0.1% SDS, 0.1% sodium deoxycholate) buffer and lysed for 10 min on ice. Lysates were centrifuged for 12 min at 4°C. Supernatants were then separated on 15% polyacrylamide SDS-PAGE gels and transferred to a PVDF membrane. The membrane was blocked in TBST (50 mM Tris-Cl, pH 7.6, 150 mM NaCl, 1% Tween 20) + 3% BSA and incubated overnight at 4°C with primary antibody LC3A/B diluted in blocking buffer. Blots were incubated with HRP conjugated to secondary antibody (Thermo Scientific, USA) and protein detected using enhanced chemiluminescence (Thermo Scientific, USA). The blot was striped with striping buffer (0.1M glycine 0.1% SDS 1% Tween20, pH to 2.2) and reproved with GAPDH antibody.

Acknowledgment

We are thankful to Patanjali Research Foundation Trust, Haridwar, India for financial support. The authors thankful to Dr. Kiran Ambatipudi and Prof. P. Roy, Dept. of Biotechnology, IIT Roorkee, for providing lab facility for conducting experiments. We are also thankful to the Central Building Research Institute (CBRI) under the Council of Scientific and Industrial Research, India for FESEM-EDX analysis. We would like thank to Toshniwal Brothers (SR) Pvt. Ltd., India for providing the facility of Raman spectroscopy. We thank Mr. Nantu Dogra, SMST, IIT-Kharagpur for repeating FTIR and few cell culture experiment to check reproducibility.

Conflict of Interest

The authors declare no conflict of interest.

Author contribution

S.K.D. conceptualization, conducted Particle characterization, cell culture experiments, immunostaining, western blot, analyzed all data, manuscript writing, reviewing and supervised overall studies; A. J. conducted the immunocytochemistry, Flow Cytometry study, analyzed the

592 data and manuscript writing; V.S. Prepared Bhasma, Particle characterization (particle
593 SEM+EDEX) manuscript writing and reviewing; L.B. assisted cell experiment, cell staining
594 procedure and western blot; N.D. performed particle charge, N.S. performed FTIR; S.S. made
595 movie from pictures of time lapse microscopy; D.M. helped for immunocytochemistry; K. J.
596 prepared cell sections for SEM; A.B. helped for Ayrvedic conceptualization, S.D. Checked all
597 data, reproducibility and review manuscript.
598

599 ## References

600 1. Henics T, Wheatley DN. Cytoplasmic vacuolation, adaptation and cell death: a view on
601 new perspectives and features. Biol Cell. **1999**, 91, 485-498.
602 2. Aki T, Nara A, Uemura K. Cytoplasmic vacuolization during exposure to drugs and other
603 substances. Cell Biol Toxicol. **2012**, 28, 125-131.
604 3. Papini E, de Bernard M, Milia E, Bugnoli M, Zerial M, Rappuoli R et al. Cellular
605 vacuoles induced by Helicobacter pylori originate from late endosomal compartments.
606 Montecucco, Proc Natl Acad Sci. **1994**, 91, 9720–9724.
607 4. Shubin AV, Demidyuk IV, Lunina NA, Komissarov AA, Roschina MP, Leonova OG et
608 al. Protease 3C of hepatitis A virus induces vacuolization of lysosomal/endosomal
609 organelles and caspase-independent cell death. BMC Cell Biol. **2015**, 16, 1-18. doi:
610 10.1186/s12860-015-0050-z.
611 5. Rogers-Cotrone T, Burgess MP, Hancock SH, Hinckley J, Lowe K, Ehrich MF et al.
612 Vacuolation of sensory ganglion neuron cytoplasm in rats with long-term exposure to
613 organophosphates. Toxicol Pathol. **2010**, 38, 554-559.
614 6. Zhang FJ, Yang JY, Mou YH, Sun BS, Wang JM, Wu CF. Oligomer procyanidins from
615 grape seeds induce a paraptosis-like programmed cell death in human glioblastoma U-87
616 cells. Pharm Biol. **2010**, 48, 883-890.

7. Korsnes MS, Espenes A. Hetland DL, Hermansen LC. Paraptosis-like cell death induced by yessotoxin. Toxicol In Vitro. **2011**, 25, 1764-1770.
8. Trabbic CJ, Dietsch HM, Alexander EM, Nagy PI, Robinson MW, Overmeyer JH et al. Differential Induction of Cytoplasmic Vacuolization and Methuosis by Novel 2-Indolyl-Substituted Pyridinylpropenones. ACS Med Chem Lett. **2014**, 5, 73-77.
9. Gandin V, Pellei M, Tisato F, Porchia M, Santini C, Marzano CA. novel copper complex induces paraptosis in colon cancer cells via the activation of ER stress signalling. J Cell Mol Med. **2012**, 16, 142-151.
10. Solano JD, González-Sánchez I, Cerbón MA, Guzmán Á, Martínez-Urbina MA, Vilchis-Reyes, MA et al. The products of the reaction between 6-amine-1,3-dimethyl uracil and bis-chalcones induce cytotoxicity with massive vacuolation in HeLa cervical cancer cell line. Eur J Med Chem. **2013**, 60, 350-359.
11. Michalik M, Pierzchalska M, Pabianczyk-Kulka A, Korohoda W. Procaine-induced enhancement of fluid-phase endocytosis and inhibition of exocytosis in human skin fibroblasts. Eur J Pharmacol. **2003**, 475, 1-10.
12. Ohkuma S, Poole B. Cytoplasmic vacuolation of mouse peritoneal macrophages and the uptake into lysosomes of weakly basic substances. J Cell Biol. **1981**, 90, 656-664.
13. Morissette G, Moreau E, Gaudreault RC, Marceau F. Massive cell vacuolization induced by organic amines such as procainamide. J Pharmacol Exp Ther. **2004**, 310, 395-406.
14. Cohen KL, Horn DLV, Edelhauser HF, Schultz RO. Effect of phenylephrine on normal and regenerated endothelial cells in cat cornea. Invest Ophthalmol Vis Sci. **1979**, 18, 242-249.

15. Karlsson HL, Nygren J, Moller L. Genotoxicity of airborne particulate matter: the role of cell-particle interaction and of substances with adduct-forming and oxidizing capacity. Mutation Res. **2004**, 565, 1-10.

16. Pool MR, Stumm J, Fulga TA, Sinning I, Dobberstein, B. Distinct modes of signal recognition particle interaction with the ribosome. Science. **2002**, 297, 1345-1348.

17. Stringer B, Imrich A, Kobzik L. Lung epithelial cell (A549) interaction with unopsonized environmental particulates: quantitation of particle-specific binding and IL-8 production. Kobzik, Exp Lung Res. **1996**, 22, 495-508.

18. Boulais J, Trost M, Landry CR, Dieckmann R, Levy ED, Soldati T et al. Molecular characterization of the evolution of phagosomes. Mol. Syst. Biol. **2010**, 6, 423. doi: 10.1038/msb.2010.80.

19. Gratton SE, Ropp PA, Pohlhaus PD, Luft JC, Madden VJ, Napier ME et al. The effect of particle design on cellular internalization pathways. PNAS. **2008**, 105, 11613-11618.

20. Blanchette CD, Woo YH, Thomas C, Shen N, Sulchek TA, Hiddessen AL. Decoupling internalization, acidification and phagosomal-endosomal/lysosomal fusion during phagocytosis of InlA coated beads in epithelial cells. PLoS One. **2009**, 4, e6056. doi: 10.1371/journal.pone.0006056.

21. Rabinovitch, M. Professional and non-professional phagocytes: an introduction. Trends Cell Biol. **1995**, 5, 85-87.

22. Claus V, Jahraus A, Tjelle T, Berg T, Kirschke H Faulstich H et al. Lysosomal enzyme trafficking between phagosomes, endosomes, and lysosomes in J774 macrophages. Enrichment of cathepsin H in early endosomes. Biol. Chem. **1998**, 273, 9842-9851.

661 23. Aderem A Underhill DM. Mechanisms of phagocytosis in macrophages. Annu. Rev.
662 Immunol. **1999**, 17, 593-623.
663 24. Rosales, C.; Uribe-Querol, E. Phagocytosis: A Fundamental Process in Immunity.
664 Biomed Res Int. **2017**, 18. doi: 10.1155/2017/9042851.
665 25. Bright, N. A.; Gratian, M. J.; Luzio, J. P. Endocytic delivery to lysosomes mediated by
666 concurrent fusion and kissing events in living cells. Curr. Biol. **2005**, 15, 360-365.
667 26. Luzio JP, Pryor PR, Bright NA. Lysosomes: fusion and function. Nat Rev Mol Cell Biol.
668 **2007**, 8, 622-632.
669 27. Desjardins, M. Biogenesis of phagolysosomes: the 'kiss and run' hypothesis. Trends Cell
670 Biol. **1995**, 5, 183-186.
671 28. Huynh KK, Grinstein S. Regulation of vacuolar pH and its modulation by some microbial
672 species. Microbiol Mol Biol Rev. **2007**, 71, 452-462.
673 29. Lukacs GL, Rotstein OD, Grinstein, S. Phagosomal acidification is mediated by a
674 vacuolar-type H(+)-ATPase in murine macrophages. J Biol Chem. **1990**, 265, 21099-
675 21107.
676 30. Shastri K. Rasatarangini of Sadanand Sharma, Motilal Banarasidas, Delhi, **2004**, 11th
677 Edi, 240.
678 31. Prakash B. Use of Metals in ayurvedic Medicine. Ind J. Hist Sci. **1997**, 32, 1-28.
679 32. The Ayurvedic Formulary of India, Government of India, New Delhi, **2003**, 2nd edi. Part
680 I.
681 33. Trikamji AY. Rasamritam, Motilal Banarasidas, Varanasi, **1951**. 6.
682 34. Vaidya PB, Vaidya BS, Vaidya SK. Response to Ayurvedic therapy in the treatment of
683 migraine without aura. Int J Ayurveda Res. **2010**, 1, 30-36.

35. Shah MR, Mehta CS, Shukla VD, Dave AR, Bhatt NN. A Clinical study of Matra Vasti and an ayurvedic indigenous compound drug in the management of Sandhigatavata (Osteoarthritis). Ayu. **2010**, 31, 210-217.

36. Shah JS, Patel JR. Anti-ulcer activity of Lucer against experimentally induced gastric ulcers in rats. Ayu. **2012**, 33, 314-316.

37. Prieto-Taboada N, Gómez-Laserna O, Martínez-Arkarazo I, Olazabal MÁ, Madariaga JM. Raman spectra of the different phases in the CaSO4-H2O system. Anal. Chemistry. **2014**, 86, 10131-10137.

38. Berenblut BJ, Dawson P, Wilkinson GR. A comparison of the Raman spectra of anhydrite ($CaSO_4$) and gypsum ($CaSO_4$).$2H_2O$). Spectrochim. Acta Part A: Molecular Spectroscopy. **1973**, 29, 29-36.

39. Sarma LP, Prasad PSR, Ravikumar N. Raman spectroscopic study of phase transitions in natural gypsumJ. Raman Spectrosc. **1998**, 29, 851-856.

40. Liu Y. Raman, mid-IR, and NIR spectroscopic study of calcium sulfates and mapping gypsum abundances in Columbus Crater, Mars. Planetary and Space Science. **2018**, 163, 35-41.

41. Sridhar DB, Gupta R, Rai B. Effect of surface coverage and chemistry on self-assembly of monolayer protected gold nanoparticles: molecular dynamics simulation study. Phys Chem Chem Phys. **2018**, 20, 25883-25891.

42. Clarke M, Engel U, Giorgione, J. Müller-Taubenberger, A.; Prassler, J.; Veltman, D et al. Curvature recognition and force generation in phagocytosis. BMC Biology. **2010**, 8, 154. doi: 10.1186/1741-7007-8-154.

43. Rougerie P, Miskolci V, Cox D. Generation of membrane structures during phagocytosis and chemotaxis of macrophages: role and regulation of the actin cytoskeleton. Immunol Rev. **2013**, 256, 222-239.
44. Wang C, Zhao T, Li Y, Huang G, White MA, Gao J. Investigation of endosome and lysosome biology by ultra pH-sensitive nanoprobes. Adv Drug Deliv Rev. **2017**, 113, 87-96.
45. Uribe-Querol E, Rosales C. Control of Phagocytosis by Microbial Pathogens. Front Immunol. **2017**, 8, 1368. doi: 10.3389/fimmu.2017.01368.
46. Mandal PK, Mandal TK Anion water in gypsum ($CaSO_4 \cdot 2H_2O$) and hemihydrate ($CaSO_4 \cdot 1/2H_2O$). Cement and Concrete Research. **2002**, 32, 313-316.
47. Pal D, Sahu CK, Haldar A. *Bhasma*: The ancient Indian nanomedicine. J Adv Pharm Technol Res. **2014**, 5, 4-12.
48. Fröhlich E. The role of surface charge in cellular uptake and cytotoxicity of medical nanoparticles. Int J Nanomedicine. **2017**, **7**, 5577-5591.
49. Blanco E, Shen H, Ferrari M. Principles of nanoparticle design for overcoming biological barriers to drug delivery. Nat Biotechnol. **2015**, 33, 941-951.
50. Alva-Murillo N, López-Meza JE, Ochoa-Zarzosa A. Nonprofessional Phagocytic Cell Receptors Involved in Staphylococcus Aureus Internalization. BioMed Research International. **2014**, 9 pages. http://dx.doi.org/10.1155/2014/538546.
51. Mollenhauer HH, Morré DJ, Rowe LD. Alteration of intracellular traffic by monensin; mechanism, specificity and relationship to toxicity. Biochim Biophys Acta. **1990**, 1031, 225-246.

52. Wada S; Kantha S, Yamashita T, Matsunaga S, Fusetani N, Watabe S. Accumulation of H+ in vacuoles induced by a marine peptide toxin, theonellamide F, in rat embryonic 3Y1 fibroblasts. Marine Biotechnology. **2002**, 4, 571-582.

53. Florey O, Gammoh N, Kim SE, Jiang X, Overholtzer M. V-ATPase and osmotic imbalances activate endolysosomal LC3 lipidation. Autophagy. **2015,** 11, 88–99.

54. Iwai-Kanai E, Yuan H, Huang C, Sayen MR, Perry-Garza CN, Kim L. Gottlieb RA. A method to measure cardiac autophagic flux in vivo. Autophagy. **2008**, **4**, 322-329.

55. Mauthe M, Orhon I, Rocchi C, Zhou X, Luhr M, Hijlkema KJ et al. Chloroquine inhibits autophagic flux by decreasing autophagosome-lysosome fusion. Autophagy. **2018**, 14, 1435-1455.

56. Lundborg, M, Lind B, Camner P. Ability of Rabbit Alveolar Macrophages to Dissolve Metals. Exp.Lung Res. **1984**, 7, 11-12.

57. Bouzas-Rodríguez J, Zárraga-Granados G, Del Rayo Sánchez-Carbente M, Rodríguez-Valentín R, Gracida X, Anell-Rendón D et al. The nuclear receptor NR4A1 induces a form of cell death dependent on autophagy in mammalian cells. PLoS One. **2015,** 10, e0118718. doi: 10.1371/journal.pone.0118718.

58. Li XZ, Sui CY, Chen Q, Chen X,P, Zhang H, Zhou XP. Promotion of autophagy at the maturation step by IL-6 is associated with the sustained mitogen-activated protein kinase/extracellular signal-regulated kinase activity. Mol Cell Biochem. **2013**, 380, 219-227.

59. Overmeyer JH, Kaul A, Johnson EE, Maltese WA. Active ras triggers death in glioblastoma cells through hyperstimulation of macropinocytosis. Mol Cancer Res. **2008**, 6, 965-977.

60. Sperandio S, Poksay K, de Belle I, Lafuente MJ, Liu B, Nasir J. Paraptosis: mediation by MAP kinases and inhibition by AIP-1/Alix. Cell Death Differ. **2004**, 11, 1066-1075.

61. Weerasinghe P, Buja LM. Oncosis: an important non-apoptotic mode of cell death. Exp Mol Pathol. **2012**, 93, 302-308.

62. Christofferson DE, Yuan J. Necroptosis as an alternative form of programmed cell death. PLoS One. **2010**, 22, 263-268.

63. Shubin AV, Demidyuk IV, Komissarov AA, Rafieva LM, Kostrov SV. Cytoplasmic vacuolization in cell death and survival. Oncotarget. **2016**, **7**, 55863-55889.

64. Overmeyer JH, Young AM, Bhanot H, Maltese WA. A chalcone-related small molecule that induces methuosis, a novel form of non-apoptotic cell death, in glioblastoma cells. Mol Cancer. **2011**, 10, 69. doi: 10.1186/1476-4598-10-69.

65. Kannan TR, Krishnan M, Ramasamy K, Becker A, Pakhomova ON, Hart PJ et al. Functional mapping of community-acquired respiratory distress syndrome (CARDS) toxin of Mycoplasma pneumoniae defines regions with ADP-ribosyltransferase, vacuolating and receptor-binding activities. Mol Microbiol. **2014**, 93, 568-581.

66. Tanida I, Ueno T, Kominami. LC3 and Autophagy. Methods Mol Biol. **2008**, 445, 77-88.

67. Rui, H.; Wei, L. Identifying an essential role of nuclear LC3 for autophagy. Autophagy. **2015**, 11, 852–853.

68. Kraft LJ, Manral P, Dowler J, Kenworthy AK. Nuclear LC3 associates with slowly diffusing complexes that survey the nucleolus. Traffic. **2016**, 17, 369–399.

Figures and Legends

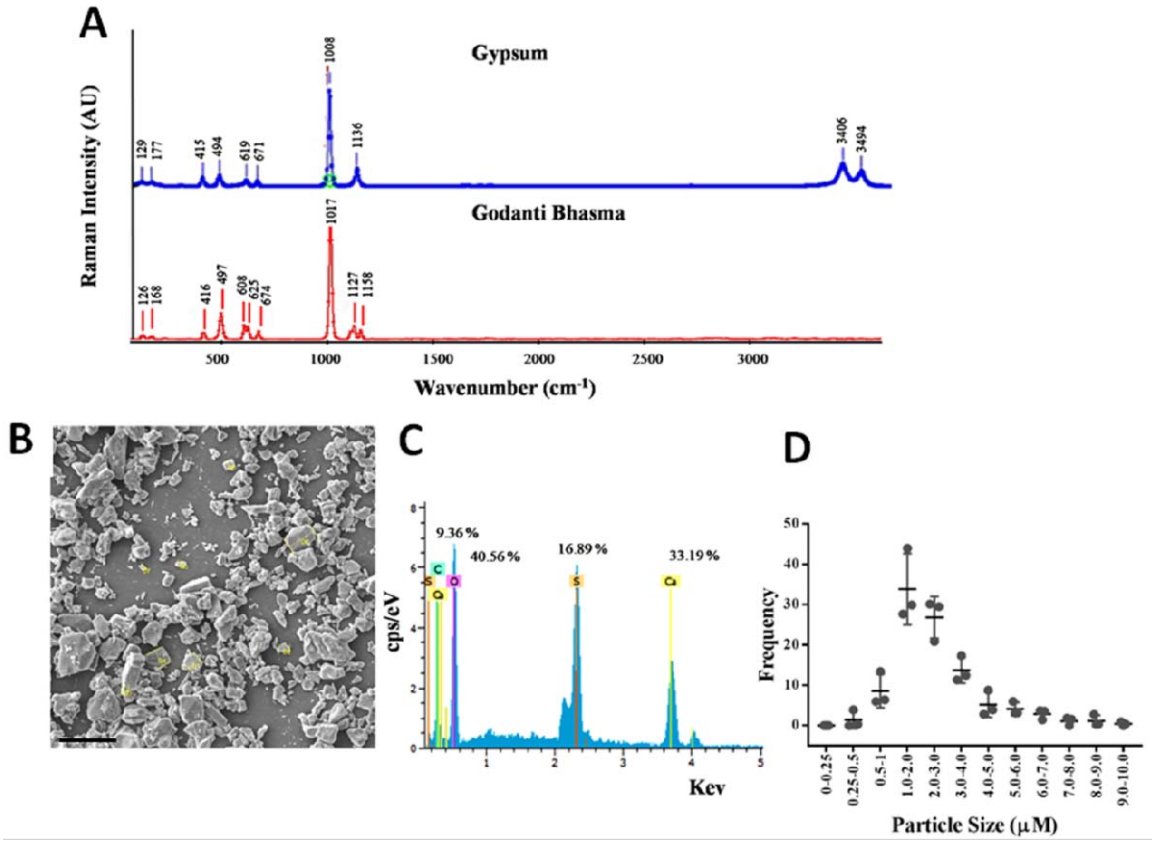

Fig. 1: Characterization of gypsum and Godanti Bhasma

(A) Raman spectra of Gypsum and Godanti bhasma. The Godanti bhasma (GB) is anhydrous calcium sulphate produced by thermal transformation of gypsum. Raman spectra showing two water molecules were disappeared in Godanti Bhasma. The spectral shifts were observed clearly between the two compounds. **(B)** Field Emission Scanning Electron Microscopy (FESEM) image showing irregular particles sizes, Scale bar = 20 µm. **(C)** Compositional analysis and weight percentage (O, Ca and S) of particles calculated from Energy-dispersive X-ray spectroscopy (EDX). **(D)** Histograms showing particle size distribution based on three independent FESEM images (mean ±SEM).

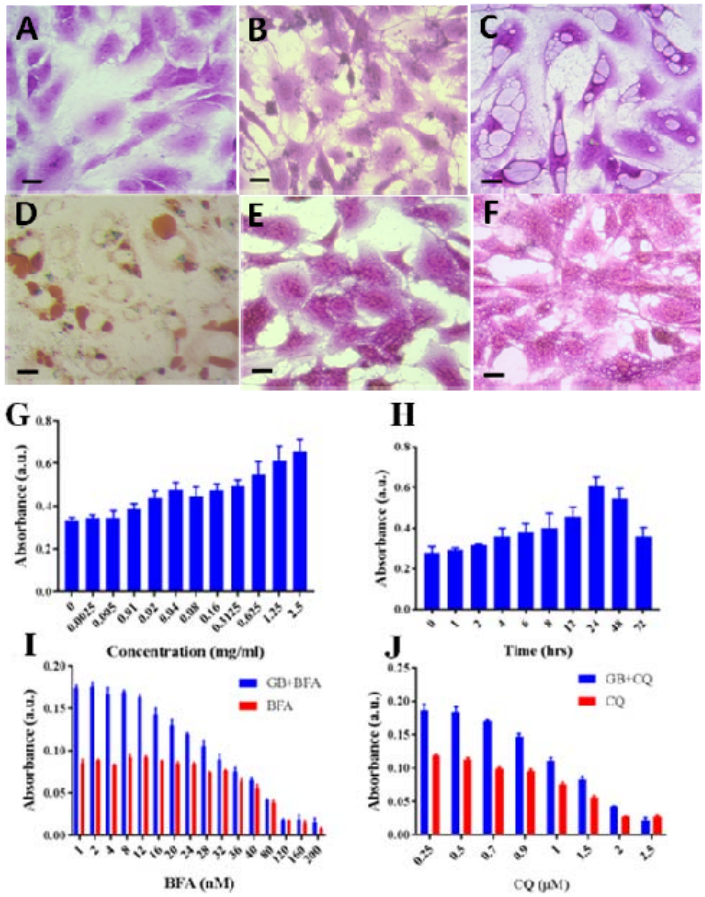

Fig. 2: Vacuole biogenesis in 3T3-L1 cells. (A) Untreated cells, **(B)** Gypsum treated cells showing no vacuoles, **(C)** Godanti Bhasma treated (0.15 mg/ml) cells showing vacuolar structure in the cytoplasm of cells; **(D)** GB treated cells stained with Neutral red showing acidic pH inside the vacuole. **(E)** Co-treatment of cells with GB (0.15 mg/ml) and BFA1 (100 nM), (**F**) Co-treatment of cells with GB (0.15 mg/ml) and CQ (2 μM). Both vacuole inhibitors suppress vacuolation. Cells were stained with Crystal violet and images were captured by a bright field microscope. (Scale bar = 20 μm) **(G)** The dose response experiment showing vacuolation increased with increasing concentration of GB treatment, **(H)** GB induced vacuolation increased with increasing times upto 24 h, **(I)** Cells were treated with GB+BFA1 and BFA1 alone. BFA1 prevents lysosome and vacuolar pH by blocking V-ATPase on their membrane. **(J)** Treatment of cells with GB+CQ and CQ alone. CQ trapped inside vacuole and increased vacuolar pH. GB was used in 0.15 mg/ml, whereas BFA1 and CQ were used in different concentrations. The results (G-J) are presented as the mean ± SD (n=6).

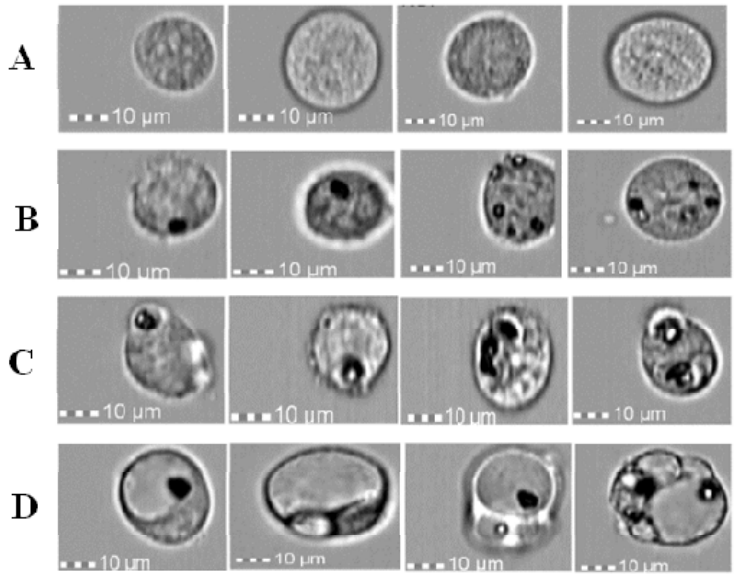

Fig. 3: Flow Cytometry cell images at dfferent time points after GB treatment. Cells at different time points (30 min-12 h) were trypsinized and run in Flow cytometry, Single-cell images were collected from Amnis Flow cytometer Image gallery at different time points. **(A)** Untreated cells, **(B)** In 30 mins, cells showing particles are attached to the cell surface, **(C)** At 1 h, cells showing GB particle internalization by membrane invaginations or outgrowth, **(D)** Treated cells at 12 h show large vacuole containing particle.

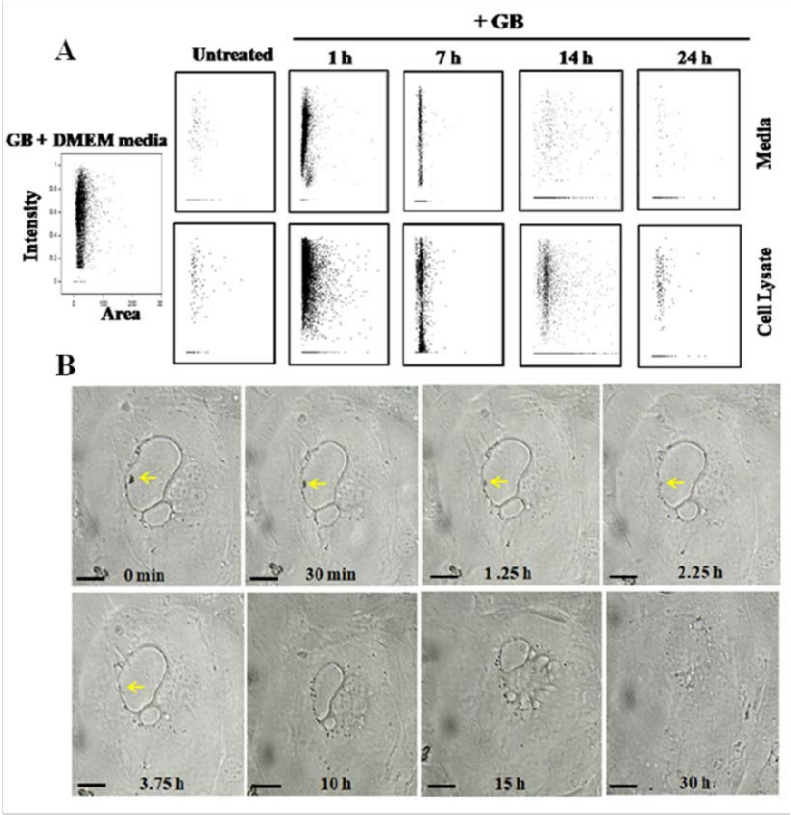

Fig. 4: GB particle degradation in 3T3-L1 cells. (a) Flow Cytometry Analysis of GB Particle in Cell Lysate and Culture Medium**.** (X-axis-brightfield area; Y-axis-bright field aspect ratio of intensity). GB particles were allowed to incubate with 3T3-L1 cells at different time periods (1, 7, 14 and 24 h) at 37 °C to internalize and following degradation. Complete DMEM containing GB particles and Untreated cells were used as control. After incubation culture media were separated from cells. Cells were lysed with RIPA buffer to release the particles; the gate was set on particles. Non-internalized particles were in culture media. Both particles in culture media and cell lysate were analyzed simultaneously by flow cytometer software (IDEAS). **(b)** Time-Lapse Microscopy of a single cell showing particle degradation inside the vacuole. Microscopic images of a single cell (GB treated) were captured and GB particle was marked with an arrow (yellow) inside the vacuole. The particle was degraded overtimes and following vacuolar turnover was also observed restoring normal morphology of cells. Images of the cell were captured in the respective times. Scale bar = 20 µm.

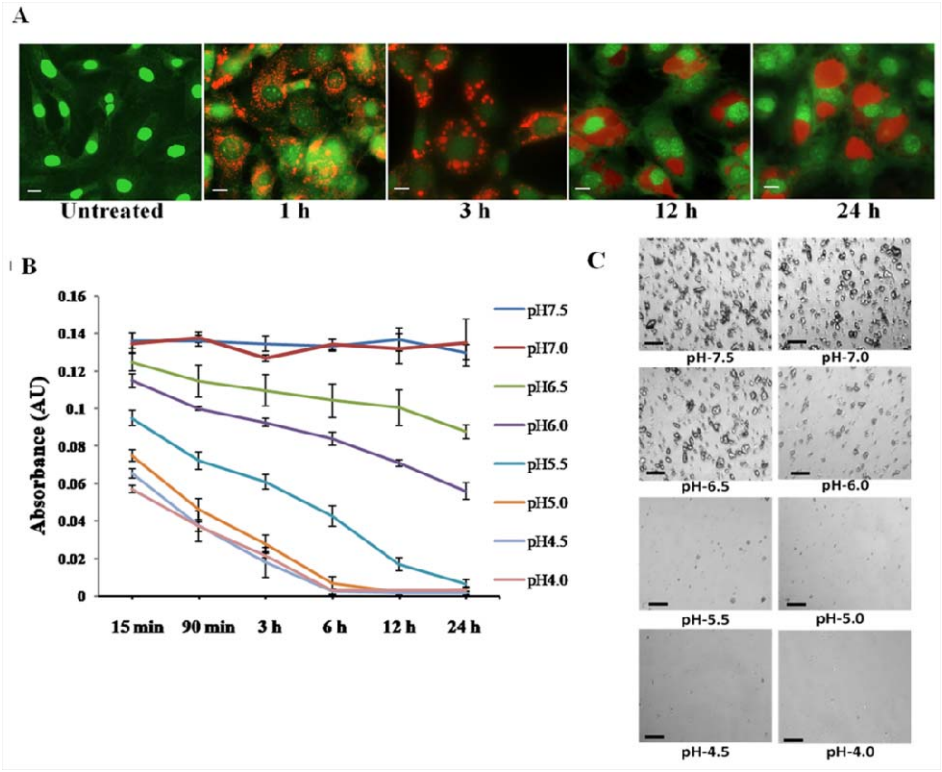

Fig. 5: Dissolution of Bhasma particle in vacuolar pH (A) Time course experiment (1h, 3h, 12h and 24 h) of GB treatment in cells. After the treatment, cells were treated with Acridine Orange showing stained (orange-red) vacuole that maintained acidic environment. Acridine orange crosses into lysosomes and becomes protonated resulting orange-red colored vacuole in treated cells, whereas in untreated cell it emits green color. The nucleus of each cell was stained as green. **(B)** The GB particles were treated in PBS buffer with different pH (4-7.5) and at different time intervals (15 min to 24 h). Turbidity test was done after specific times. At physiological pH (7 and 7.5) GB particles were not soluble, whereas the particles were gradually soluble with decreasing pH (Lysosomal/vacuolar pH; 6.5 to 4.5). The pH 5 showed the lowest solubility which is mimicking acidic vacuolar environment. The results are presented as the mean ± SD (n=6). **(C)** Microscopic images of GB particles at different pH after 24 h.

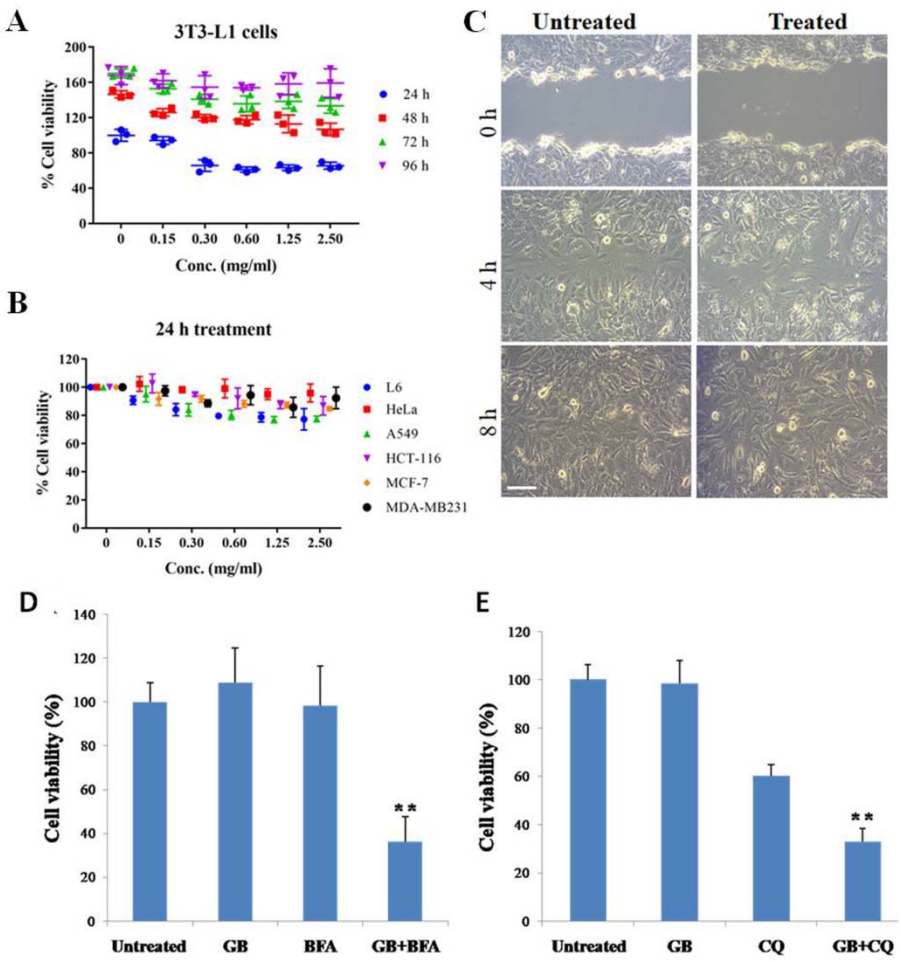

Fig. 6: Effect of Godanti Bhasma on Cell Viability and Proliferation. (A) Cell viability in 3T3-L1 at different time points (24, 48, 72 and 96 h) at concentration ranges from 0-2.5 mg/ml using MTT assay **(B)** Cell viability in L6, Neuro 2a, HeLa, MDA-MB231, A549, HCT 116 and MCF-7 at concentrations vary from 0 – 2.5 mg/ml after 24 h of treatment using MTT assay, **(C)** Scratch assay in Bhasma treated 3T3L1 cell at different time points (0, 4 and 8 h). The cells were viable and proliferation was normal. , Scale bar = 50 µm. **(D)** Loss of viability of GB induced vacuolated cell by post treatment of Vacuole inhibitor BFA1 with controls, and **(E)** Loss of viability of GB induced vacuolated cell by Post treatment of CQ in GB treated cells with controls. A significant toxicity of GB induced vacuolated cells was observed by the post treatment of BFA1/CQ compared to GB and BFA1/CQ controls. The concentration of GB, BFA1 and CQ were 0.3 mg/ml, 100 nM and 1 µM respectively. $^{**}P < 0.01$. The results are presented as the mean ± SD (n=6).

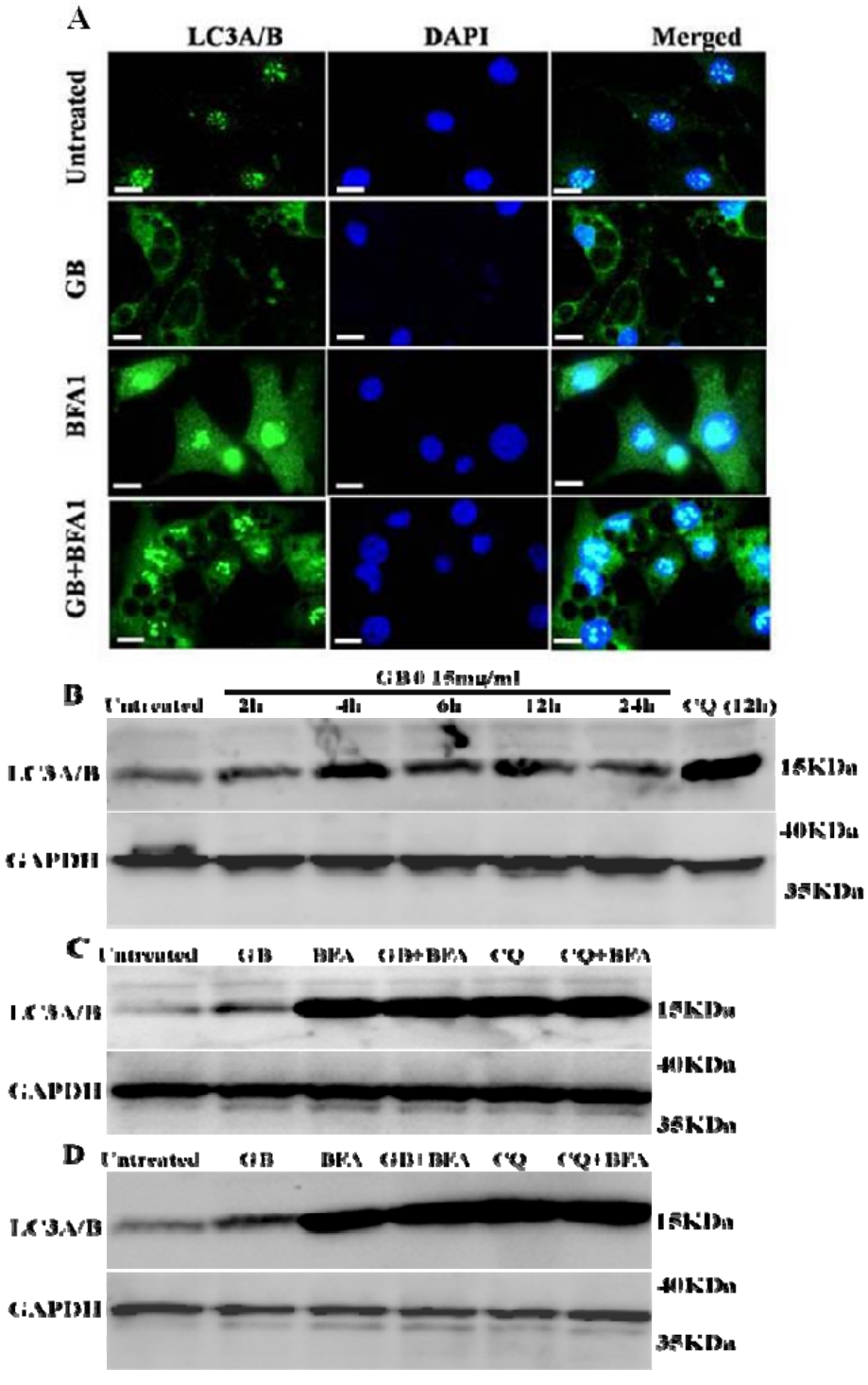

969 **Fig. 7: GB activated LAP like function.** (A) Fluorescence image (40X) of Immuno-staining
970 with LC3 A/B antibody showing LC3 expression in 3T3L1, LC3 expressed within nucleus in
971 untreated cells, whereas in GB treatment, LC3 expression was found in membrane/ periphery of
972 vacuoles indicating presence of LAP like function. LC3 expression in BFA treated cells showing
973 LC3 expression in whole cell, and In GB+BFA, the post treatment of BFA was done in GB
974 induced vacuolated cells, showing absence of LC3 (LC3-II) accumulation on vacuolar membrane
975 indicating LAP like function was suppressed, whoever expression was present in whole cell. (B)
976 The western blot showing expression of LC3 in 3T3L1 cells in different time points showing
977 LC3 expression was in steady state compared to untreated and CQ treatment. Untreated cells was
978 showing very less expression whereas CQ High expression, (C) Showing LC3 expression by the
979 treatment of GB with or without autophagy inhibitors (BFA and CQ), BFA and CQ inhibited of
980 vacuolar function as well as autophagy flux, and (D) Neuro2a experiment same as of (C).
981 Vacuole inhibitors BFA and CQ abolished the LAP function in cells by inhibition of vacuolar
982 function as well as autophagy flux. Scale bar = 20 µm.
983